International Symposium
On Turbulence and Shear Flow
Phenomena (TSFP-9)
June 30 - July 3, 2015 Melbourne, Australia

SKIN-FRICTION BEHAVIOR IN THE TRANSITIONALLY-ROUGH REGIME

Karen A. Flack[1], Michael P. Schultz[2], Julio M. Barros[1], Yechan C. Kim[2]
Department of Mechanical Engineering[1]
Department of Naval Architecture and Ocean Engineering[2]
United States Naval Academy
Annapolis, MD 21402 USA
flack@usna.edu, mschultz@usna.edu, barros@usna.edu

ABSTRACT

Results of an experimental investigation of the skin friction for a range of rough surfaces in fully-developed, turbulent channel flow are presented. The fifteen surfaces were generated by grit blasting with various types and sizes of media. The Reynolds number (Re_m) for the experiments based on the bulk mean velocity and the channel height spanned from 10,000 – 300,000. The root-mean-square roughness height (k_{rms}) is shown to be most strongly correlated with the equivalent sand roughness height (k_s) for the grit-blasted surfaces. The shape of the roughness function (ΔU^+) for all of these surfaces shows self-similarity. The roughness function displays inflectional behavior in the transitionally-rough regime in a similar manner to the results of Nikuradse for uniform sand. The equivalent sand grain roughness height can be predicted using k_{rms} and the skewness (S_k) of the probability density function of the roughness amplitude. A long-wavelength filtering procedure based on the Taylor microscale (λ) of the roughness is presented, and it is recommended that roughness profiles be filtered at a scale of at least 50λ.

INTRODUCTION

The behavior of wall-bounded flows over roughness is a great interest to both scientists and engineers because of the role roughness plays in altering momentum and heat transfer. Excellent reviews on roughness effects on turbulent flows are given by Raupach *et al.*[1] and Jimenez[2]. From a practical perspective, one of the primary shortcomings in the understanding of roughness effects is identifying the relationship between the surface texture and the resulting skin friction.

Since roughness can influence the skin friction in a range of flow types including internal (e.g. pipes and ducts) and external (e.g. boundary layers) flows, it is useful to introduce a function that allows direct comparison among these different geometries[3]. The roughness function (ΔU^+) introduced in 1954 separately by Clauser[4] and Hama[5] does this. In the overlap region of a wall-bounded turbulent flow between the inner layer and the outer layer, the mean flow is well described by the log law as follows

$$U^+ = \frac{1}{\kappa}\ln y^+ + B, \qquad (1)$$

where U^+ is the mean streamwise velocity normalized by the friction velocity, κ is the von Karman constant, y^+ is the distance from the wall normalized by the viscous length scale, and B is the smooth-wall additive constant. Wall roughness can increase the momentum deficit in the overlap region of the boundary layer. The effect is a downward shift in the log law. This shift is called the roughness function. Therefore, the mean flow in the overlap region for rough-wall flows can be written as

$$U^+ = \frac{1}{\kappa}\ln y^+ + B - \Delta U^+. \qquad (2)$$

Figure 1 illustrates two classic roughness function types versus roughness Reynolds number based on the equivalent sand roughness height (k_s^+). These are the Nikuradse-type[6] and Colebrook-type[7] roughness functions. As can be seen in figure 1, when the roughness Reynolds number is small ($k_s^+ <$ ~5)[8] the Nikuradse-type roughness has ΔU^+ equal to zero. This is the hydraulically-smooth flow regime. It can be physically interpreted as a condition in which any perturbation induced by the roughness elements is completely damped out by viscosity. The Colebrook-type roughness function does not strickly display a hydraulically-smooth flow regime, and $\Delta U^+ \rightarrow 0$ only in the limit as $k_s^+ \rightarrow 0$.

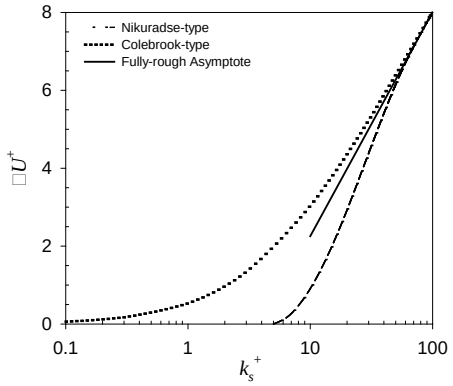

FIG. 1. The roughness function (ΔU^+) versus roughness Reynolds number (k_s^+).

In the limit of large k_s^+, form drag on the individual roughness elements becomes the dominant source of skin friction with the viscous stress becoming negligible. This is termed the fully-rough regime and is indicated when the skin-friction coefficient becomes independent of Reynolds number. In terms of ΔU^+, the fully-rough asymptote is given as follows[10]

$$\Delta U^+ = \frac{1}{\kappa}\ln k_s^+ + B - 8.5 \qquad (3)$$

As shown in Figure 1, both Nikuradse-type and Colebrook-type roughness approach the fully-rough asymptote provided k_s^+ is sufficiently large. Schlichting[11] gives the onset of fully-rough conditions for Nikuradse-type roughness to be at k_s^+ = 70. For Colebrook-type roughness, the transition to fully-rough conditions is more gradual with the approach being asymptotic at large k_s^+. For intermediate values of k_s^+, the flow is transitionally-rough. In this regime, both form drag on the roughness elements and viscous stress are significant. In the transitionally-rough regime, the Nikuradse-type roughness displays inflectional behavior indicative of a local minima in the skin-friction coefficient occurring in this range, while the Colebrook-type roughness shows monotonic variation with k_s^+. Bradshaw[10] points out that 'real-life surfaces' should behave like Colebrook-type roughness owing to the larger range of length scales present compared to the uniform sand used in Nikuradse's experiments. More recent studies of engineering roughness which cover a wide Reynolds number range do not display Colebrook-type roughness behavior but behave more similar to Nikuradse-type roughness[11,12,13].

Another topic which has been the focus of a great deal of research is relating the physical roughness topography to its effective hydraulic length scale (e.g. k_s). A review of much of the work in this area was undertaken by the present authors[14]. The focus of that study was roughness scaling in the fully-rough flow regime. All surfaces, despite possible differences in the transitionally-rough regime, approach fully-rough behavior as k_s^+ becomes sufficiently large, allowing collapse of ΔU^+ for all surfaces if k_s is properly specified (see Figure 1). This led Bradshaw[13] to term k_s a 'common currency' which is useful in comparing the effect of disparate types of roughness in the fully-rough regime. Based on results from a number of investigators for both regular and irregular roughness in the fully-rough regime, Flack and Schultz[17] found that k_s was reasonably well predicted using a correlation involving the root-mean-square roughness height (k_{rms}) and the skewness (S_k) of the surface elevation probability density function. It is of note that Musker[15] previously developed a roughness function correlation based on these same parameters in a study of what he termed 'naturally-occurring surfaces'. However, he also included the kurtosis and mean roughness slope in his correlation, but Flack and Schultz[17] found no significant improvement in their correlation by including them.

The behavior of the skin friction in the transitionally-rough flow regime is complex and for that reason more poorly understood than in the fully-rough regime. Grigson[16] reviewed skin-friction research for ship-bottom paints conducted by several investigators. The wide-ranging roughness function behavior observed in the transitionally-rough regime from the various studies led Grigson to the conclude that predicting roughness function behavior based on roughness topography alone was not promising. This points to the need for taking a systematic approach if significant progress is to be made. Recent work by the Flack *et al.*[17] focused on studying only the onset of the transitionally-rough flow regime for modern ship-bottom paints, sanded surfaces, and sandpaper. They observed that the transition from the hydraulically-smooth to the transitionally-rough flow regime occurs abruptly at a finite roughness Reynolds number more closely following Nikuradse-type than Colebrook-type roughness behavior. It was also found that the onset of the transitionally-rough regime is related to the largest roughness scales. However, the experiments did not allow the nature of the entire transitionally-rough regime to be investigated.

Although rough-wall-bounded flows have been studied extensively, several practical questions remain largely unresolved. First, the relationship between the shape of the roughness function in transitionally-rough regime and surface topography which gives rise to it are not well understood. Second, it is not completely clear which textural parameters best describe a rough surface in a hydraulic sense. Furthermore, the range of roughness wavelengths that influence the skin friction is not well understood. The focus of the present work is to attempt to address these questions with a systematic study of the skin friction of fifteen rough surfaces that were generated by grit blasting. The hydrodynamic tests were carried out over a rather large Reynolds number range. Five surfaces were prepared by grit blasting with a single scale blast media. These underwent hydrodynamic testing and were subsequently blasted with secondary and tertiary scale media in order to investigate the role that the incorporation of additional roughness length scales plays in determining the shape of the roughness function and the resulting hydraulic length scale.

EXPERIMENTAL FACILITIES AND METHODS

The present experiments were conducted in the high Reynolds number turbulent channel flow facility at the United States Naval Academy, shown in Figure 2. The test section is 25 mm in height (H), 200 mm in width (W), and 3.1 m in length (L). The bulk mean velocity in the test section ranges from 0.4 – 11.0 ms^{-1}, resulting in a Reynolds number based on the channel height and bulk mean velocity (Re_m) range from 10,000 – 300,000. Further details of the facility including flow management devices, tripping, and flow quality are given in Schultz and Flack[18]. Nine static pressure taps are located in the test section of the channel. They are 0.75 mm holes and are placed along the centerline of the side wall of the channel and are spaced 6.8H apart. Pressure taps 5 – 8 are used to measure the streamwise pressure gradient in the channel, located ~90H – 110H downstream of the trip at the inlet to the channel.

The wall shear stress, τ_w, was determined via measurement of the streamwise pressure gradient. The similarity-law procedure of Granville[19] for fully-developed internal flows was employed to determine the roughness function, ΔU^+. The flow developed over smooth walls for a distance of 60H in the upstream portion of the channel. The roughness-covered plates formed the top and bottom walls for the remainder of the test section. There was a roughness fetch of 30H before the first tap used in the determination of dP/dx. Fully-developed flow was confirmed with velocity profiles located

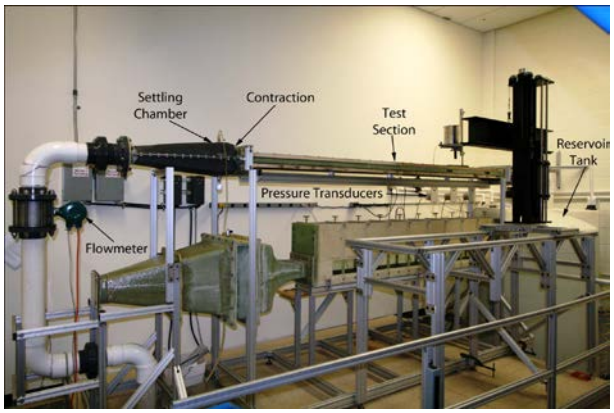

FIG. 2. High Reynolds number turbulent channel flow facility.

90*H* and 110*H* downstream of the trip. Details of the velocity measurements are outlined in Schultz and Flack[21].

The test plates were fabricated from cast acrylic sheet with roughness generated through grit blasting. Five sets of test plates were originally manufactured. Each of these sets was grit blasted with a different blast media. These included 8-12-grit crushed glass, 36-grit garnet, 25-grit steel, 46-grit aluminum oxide, and 120-grit garnet. After hydrodynamic testing of the five test surfaces, they were grit blasted with a different blast media to incorporate a secondary roughness length scale on the surface. After hydrodynamic tests of these surfaces were completed, they were again grit blasted with another blast media to impose a tertiary roughness length on the surface. This process produced 15 test surfaces with a range of surface textures. In general, the scale of the secondary and tertiary blast media used was finer than the original one so as to allow the larger scale features to persist while adding smaller scale texture. The one exception was the surface originally blasted with 120-grit garnet which was subsequently blasted with coarser media. The test surfaces that were generated along with their designations are presented in Table I with surface scans shown in Figure 3.

The surfaces scans, comprised of 60 mm by 10 mm area (*x* and *y* direction, respectively), were profiled with an optical profilometer utilizing white light interferometry (Veeco Wyco NT9100), with sub-micron vertical resolution and 3.4μm lateral resolution. The data from the profilometer usually require careful post-processing in order to remove any anomalies and spurious data as well as filling all holes in the surface scans. Prior to post-processing, all 15 surfaces had tilt and curvature removed. The post-processing steps consisted of interpolating the holes using a PDE-based interpolation method (Bertalmio et al.[20] inpainting technique commonly used in image processing where series of linear PDE's are solved in the vicinity of the holes) and, subsequently, a median-test filter was used to remove spurious data (artificial peaks and valleys that were clearly not part of the surface) followed by a second PDE-based interpolation. Lastly, a median filter with 3 × 3 kernel was employed to remove high-frequency noise in the measurements. This methodology

TABLE I. Test surface designation with blast media sequence.

	Original Blast Media	Secondary Blast Media	Tertiary Blast Media	Marker
1	8-12 grit crushed glass	NA	NA	●
2	8-12 grit crushed glass	25-grit steel	NA	△
3	8-12 grit crushed glass	25-grit steel	36-grit garnet	■
4	36-grit garnet	NA	NA	◇
5	36-grit garnet	80-grit garnet	NA	▼
6	36-grit garnet	80-grit garnet	fine glass bead	○
7	25-grit steel	NA	NA	▲
8	25-grit steel	46-grit Al oxide	NA	□
9	25-grit steel	46-grit Al oxide	80-grit garnet	◆
10	46-grit Al oxide	NA	NA	▽
11	46-grit Al oxide	120-grit garnet	NA	⊙
12	46-grit Al oxide	120-grit garnet	fine glass bead	△
13	120-grit garnet	NA	NA	⊡
14	120-grit garnet	80-grit garnet	NA	◇
15	120-grit garnet	80-grit garnet	fine glass bead	▽

NA = not applicable

ensured that the surface scans represented the actual surfaces quite accurately. In order to compute the roughness statistics, a total of 10 line-scans per surface were extracted (*x*-direction). These profiles had 1mm space between them to ensure statistical independence.

RESULTS AND DISCUSSION

Figure 4 presents sample skin-friction results as a function of Reynolds number, Re_m. Also shown for comparison are the smooth wall experimental results of Schultz and Flack[21]. Secondary blasting (surface 2) increases the surface roughness, resulting in roughness effects at lower Reynolds numbers, as compared to surface 1. Additional blasting with a finer media (surface 3) does not significantly change the skin-friction, actually slightly reducing the frictional drag. This may be due to the additional grit blasting modifying the larger scale features. All three surfaces eventually reach fully rough behavior at sufficient Re_m, indicated by a constant C_f.

The roughness function (ΔU^+) is shown in figure 5 as a function of the roughness Reynolds number (k_s^+). The roughness function for the grit blasted surfaces show fairly good collapse when scaled using k_s, indicating that grit blasting produces similar roughness features, even with the inclusion of additional scales. For $k_s^+ < \sim 3$, these surfaces are hydraulically-smooth ($\Delta U^+ \equiv 0$). The roughness function shows inflectional behavior in the transitionally-rough flow regime. The onset of the fully-rough regime is observed at $k_s^+ \sim 20$. Therefore, the present results stand in contrast to the Colebrook-type roughness function which provides the

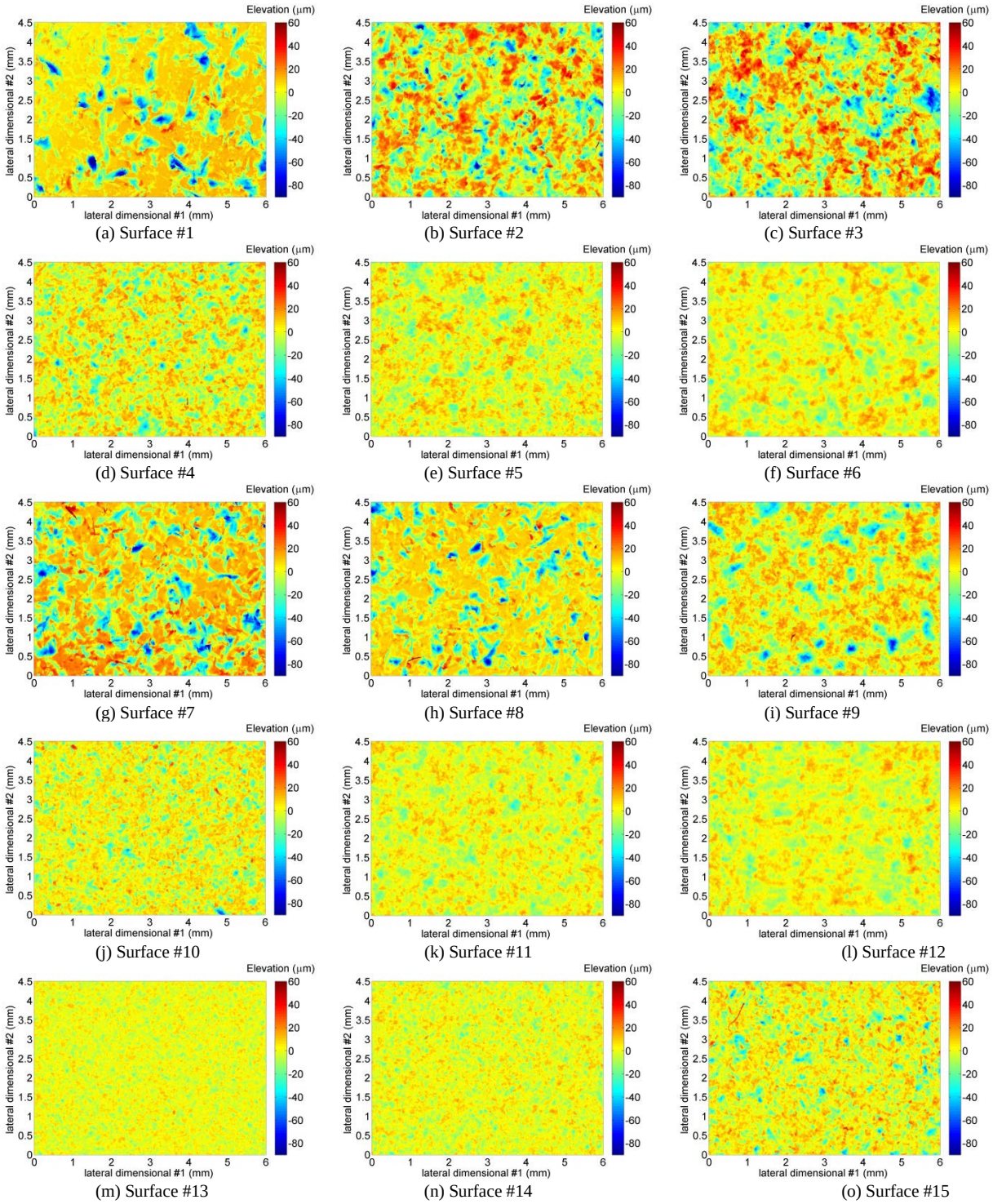

(a) Surface #1 (b) Surface #2 (c) Surface #3

(d) Surface #4 (e) Surface #5 (f) Surface #6

(g) Surface #7 (h) Surface #8 (i) Surface #9

(j) Surface #10 (k) Surface #11 (l) Surface #12

(m) Surface #13 (n) Surface #14 (o) Surface #15

FIG. 3. Surface topography maps for the 15 test surfaces, (a) – (o) represent surfaces #1-15, respectively. The maps are of 6 mm by 4.5 mm sections of the surface, and the vertical colorbar for surface elevation ranges from -90 μm to 60 μm for all the surfaces.

TABLE II. Surface statistics and surface parameters

	k_{rms} [μm]	S_k	K_u	Taylor [μm]	k_s actual [μm]	k_s=f (k_{rms},S_k) predicted (eqn 3) [μm]
1	18.91	-0.80	3.95	36.60	37.50	51.62
2	19.87	-0.71	3.88	36.76	52.40	56.54
3	19.59	-0.39	3.64	36.95	49.50	49.94
4	10.24	-0.40	3.53	28.99	29.60	51.57
5	9.22	-0.36	3.44	27.65	29.10	53.17
6	8.01	-0.73	4.11	34.52	20.00	49.29
7	18.03	-1.27	5.38	35.25	58.30	25.81
8	15.88	-1.51	5.62	36.88	56.30	23.08
9	16.85	-0.73	3.62	44.38	43.00	21.51
10	9.14	-1.02	5.57	24.73	36.60	56.63
11	9.57	-0.21	3.01	30.54	24.30	55.76
12	9.27	-0.14	3.17	36.63	22.60	45.32
13	6.62	0.66	15.7	18.41	15.70	26.39
14	6.71	-0.41	3.74	22.36	23.50	23.35
15	11.89	-0.68	3.91	28.13	35.00	22.37

foundation for the Moody diagram. These results and those of several other recent studies[11,12,13] seem to indicate the skin-friction behavior observed by Nikuradse was not an anomaly due to the narrow range of roughness length scales present in the uniform sand roughness but is in fact far more common for engineering roughness than previously presumed.

Flack and Schultz[17] developed a new roughness correlation for the fully-rough regime that is based upon roughness parameters. In this correlation, the equivalent sandgrain roughness height, k_s, is a function of the root-mean-square roughness, k_{rms}, and the roughness skewness, S_k, The correlation worked well for a range of different rough surfaces. Although this correlation was "tuned" for surfaces that mainly possess positive S_k it, nonetheless, provides a framework to study the grit-blasted surfaces which are negatively skewed due to the surface manufacturing technique. A form of the correlation by Flack and Schultz[17] was used to investigate how well k_s is predicted by the roughness parameters (k_{rms} and S_k) for the grit blasted surfaces. Figure 6 shows the results for the correlation listed below.

$$k_s = f(k_{rms}, S_k) \approx 2.87 k_{rms}(2 + S_k)^{-0.28} \qquad (4)$$

Due to the fact that the surfaces studied in this work have negative skewness, the additive constant is set to 2, in contrast to Flack and Schultz[17]. Regardless of the additive constant, this model seems to adequately predict k_s. Figure 5 also shows the linear correlation between the predicted values of k_s and the actual, measured, k_s, providing a goodness of the fit of R^2 = 0.882.

It is also important to parametrically investigate the affect that filtering has on the roughness statistics[21,22]. Instead of choosing a cut-off length scale based on an arbitrary quantity, for example a 2mm cut-off, it is more reasonable to choose one that is related in some way to the surface statistics. Yuan and Piomelli[23] introduced the concept of the roughness Taylor

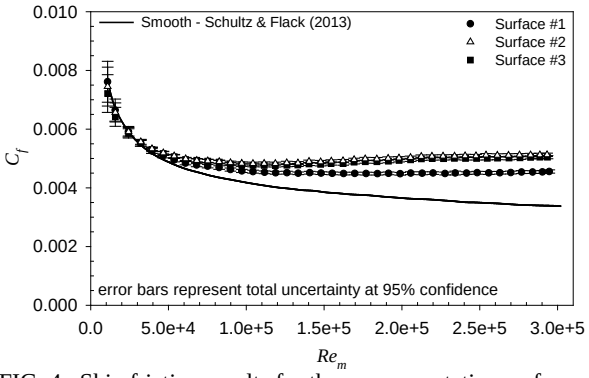

FIG. 4. Skin friction results for three representative surfaces.

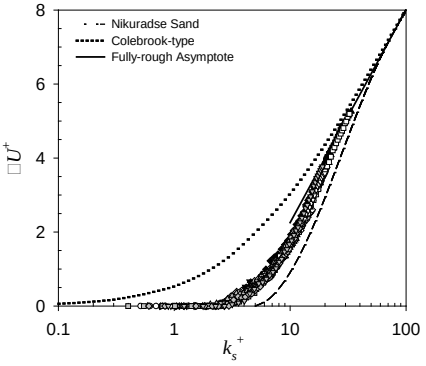

FIG. 5. Roughness function results all surfaces.

microscale, λ, where this quantity represents the average size of the roughness elements that constitute the rough-surface, and therefore the size of the elements that would contribute the most to the drag. For this reason, the roughness Taylor microscale seems to be a good candidate for the cut-off length scale. Herein, the roughness Taylor microscale is defined as (in contrast to the parabolic fit used in Yuan and Pilomelli[23])

$$\lambda^2 = \frac{z^2}{\langle (\frac{dz}{dx})^2 \rangle} \qquad (4)$$

where z is the surface root-mean-square and dz/dx is the surface gradient in the x-direction. In order to systematically remove wavelengths that contribute little to drag, but nonetheless greatly affect the roughness statistics[21,22], a multiple of the roughness Taylor microscale ($N \times \lambda$, where N is an integer value) was used to define the cut-off length scale for the high-pass filter. By employing this methodology, the filter's cut-off length scale is dependent entirely upon the roughness statistics and varies across all the different surfaces studied. The high-pass filtered roughness statistics were then input in the model proposed by Flack and Schultz[17], where the coefficients of the equation were estimated via an unconstrained nonlinear optimization least-square fit. Several cut-off lengths were tested. Figure 7 shows the correlation coefficient as a function of the number of Taylor microscales. The highest correlation plateaus at ~20λ with a very gradual drop off with increased filter size. It is of note that the correlation drops rather precipitously for filter sizes smaller than 20λ. This indicates that relevant topographical information is discarded if the filter is set to be smaller than ~20λ. While the unfiltered grit blasted surfaces yielded a high

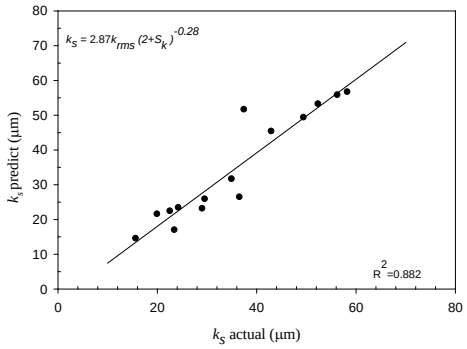

FIG. 6. k_s predicted vs k_s actual for unfiltered surface data.

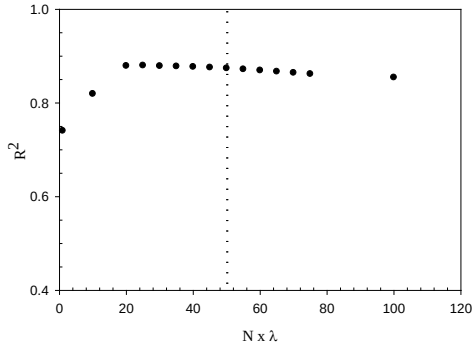

FIG. 7. Goodness of fit vs number of Taylor microscales

correlation coefficient, real engineering surfaces which were not carefully manufactured in the laboratory will likely require a long-wavelength filter to remove undulations and surface curvature that influence the surface statistics but do not contribute to the surface drag. Guided by the present results, it is recommended that a long-wavelength filter size of at least 50λ is used before calculating the surface statistics. For the grit blasted surfaces, the roughness Taylor microscope ranged from ~18μm to ~50μm, which gives a cut-off high-pass filter length scale ranging from ~1mm to ~2mm. With a 50λ filter the correlation equation becomes:

$$k_s = f(k_{rms}, S_k) \approx 3.93 k_{rms}(2 + S_k)^{-0.40} \qquad (5)$$

CONCLUSIONS

The skin-friction of rough surfaces generated by grit blasting was measured over a wide Reynolds number range. The shape of the roughness function (ΔU^+) for all of these surfaces shows self-similarity. The root-mean-square roughness height (k_{rms}) was shown to be most strongly correlated with the equivalent sand roughness (k_s).

The roughness function displays inflectional behavior in the transitionally-rough regime. This is analogous to the results of Nikuradse for uniform sand although the onset of roughness effects and the approach to fully-rough conditions both occur at smaller roughness Reynolds number (k_s^+). These results stand in contrast to the often-assumed, monotonic, Colebrook-type roughness function on which the Moody diagram is based, in agreement based a and results are consistent with other recent studies. The roughness correlation developed by Flack and Schultz[17] was used, with a modified additive constant, to predict k_s, based on k_{rms} and S_k. There was good agreement between the resulting predicted k_s and the actual k_s obtained in the experiments (R^2 = 0.882). A methodology for post-processing the profiled rough surfaces was also presented. Filtering roughness profiles based upon the roughness Taylor microscale (λ) is suggested. Specifically, a long-wavelength filter of 50λ appears to remove undulations that do not significantly contribute to the skin-friction. Although grit-blasted results were presented here, the roughness statistics could not be controlled in a systematic fashion. Controlling these parameters would appear to be critical to understanding the behavior of drag on rough surfaces. Currently, we are investigating roughness that is mathematically generated, where the roughness statistics can be systematically changed and controlled to identify which roughness scales contribute the most to frictional drag.

REFERENCES

[1] M. R. Raupach, R. A. Antonia, and S. Rajagopalan, "Rough-wall turbulent boundary layers," *Appl. Mech. Rev.* 44, 1-25 (1991).

[2] J. Jimenez, "Turbulent flows over rough walls," *Annu. Rev. Fluid Mech.* **36**, 173–196 (2004).

[3] M. P. Schultz and A. Myers, "Comparison of three roughness function determination methods," *Exps. Fluids* **35**, 372-379 (2003).

[4] F. H. Clauser, "The turbulent boundary layer in adverse pressure gradients," *J. Aero. Sci*. **21**, 333-358 (1954).

[5] F. R. Hama, "Boundary–layer characteristics for smooth and rough surfaces," *Trans Soc. Naval Archit. Mar. Engrs* **62**, 333-358 (1954).

[6] J. Nikuradse, "Laws of flow in rough pipes," *NACA Tech. Memo*. TM1292 (1933).

[7] C. F. Colebrook, "Turbulent flow in pipes with particular reference to the transition region between the smooth and rough pipe laws," *J. Inst. Civil Engrs* **11**, 133-156 (1939).

[8] H. Schlichting, Boundary-Layer Theory. 7th Ed., McGraw Hill (1979).

[9] P. M. Ligrani and R. J. Moffat, "Structure of transitionally rough and fully rough turbulent boundary layers," *J. Fluid Mech.* **162**, 69-98 (1986).

[10] P. Bradshaw, "A note on "critical roughness height" and "transitional roughness"," *Phys. Fluids* **12**, 1611-1614 (2000).

[11] M. A. Shockling, J. J. Allen, and A. J. Smits, "Roughness effects in turbulent pipe flow," *J. Fluid Mech.* **564**, 267-285 (2006).

[12] M. P. Schultz and K. A. Flack, "The rough-wall turbulent boundary layer from the hydraulically smooth to the fully rough regime," *J. Fluid Mech.* **580**, 381-405 (2007).

[13] L. I. Langelandsvik, G. J. Kunkel, and A. J. Smits, "Flow in commercial steel pipe," *J. Fluid Mech.* **596**, 323-339 (2008).

[14] K. A. Flack and M. P. Schultz, "Review of hydraulic roughness scales in the fully rough regime," *Trans. ASME - J. Fluid Eng.* **132**, 041203 (2010).

[15] A. J. Musker, "Universal roughness functions for naturally-occurring surfaces," *Trans. Can. Soc. Mech. Eng.* **1**, 1-6 (1980-1981).

[16] C. Grigson, "Drag losses of new ships caused by hull finish," *J. Ship Res.* **36**, 182-196 (1992).

[17] K. A. Flack, M. P. Schultz, and W. B. Rose, "The onset of roughness effects in the transitionally rough regime," *Int. J. Heat and Fluid Flow* **35**, 160-167 (2012).

[18] M.P. Schultz and K. A. Flack, "Reynolds-number scaling of turbulent channel flow," *Phys. Fluids* **25**, 025104 (2013).

[19] P.S. Granville, "Three indirect methods for the drag characterization of arbitrary rough surfaces on flat plates," *J. Ship Res.* **31**, 70-77 (1987).

[20] M. Bertalmino, G. Sapiro, V. Caselles and C. Ballester, "Image Impainting," 27th Conference on Computer Graphics and Interactive Techniques, ACM Press/Addison Wesley Publishing Co., 417-424 (2000).

[21] J. S. Medhurst, "Outline of a Draft International Standard for the Measurement and Characterisation of Roughness Topography in Fluid Flow," *Proceedings of the RINA International Workshop on Marine Roughness and Drag*, London, UK (1990).

[22] D. Howell and B. Behrends, "A Review of Surface Roughness in Antifouling Coatings Illustrating the Importance of Cutoff Length," *Biofouling*, **22**, 401-410 (2006).

[23] J. Yuan and U. Piomelli, "Estimation and Prediction of the roughness function on Realistic Surfaces," *J. Turb*., **15**, 350-365 (2014).